

EXPLORING THE EVOLUTIONARY PATHS OF THE MOST MASSIVE GALAXIES SINCE $Z \sim 2$

PABLO G. PÉREZ-GONZÁLEZ^{1,2}, IGNACIO TRUJILLO³, GUILLERMO BARRO¹, JESÚS GALLEGO¹, JAIME ZAMORANO¹,
CHRISTOPHER J. CONSELICE⁴

Draft version September 3, 2021

ABSTRACT

We use *Spitzer* MIPS data from the FIDEL Legacy Project in the Extended Groth Strip to analyze the stellar mass assembly of massive ($M > 10^{11} M_{\odot}$) galaxies at $z < 2$ as a function of structural parameters. We find 24 μm emission for more than 85% of the massive galaxies morphologically classified as disks, and for more than 57% of the massive systems morphologically classified as spheroids at any redshift, with about 8% of sources harboring a bright X-ray and/or infrared emitting AGN. More noticeably, $\sim 60\%$ of all compact massive galaxies at $z = 1\text{--}2$ are detected at 24 μm , even when rest-frame optical colors reveal that they are dead and evolving passively. For spheroid-like galaxies at a given stellar mass, the sizes of MIPS non-detections are smaller by a factor of ~ 1.2 in comparison with IR-bright sources. We find that disk-like massive galaxies present specific SFRs ranging from 0.04 to 0.2 Gyr^{-1} at $z < 1$ (SFRs ranging from 1 to 10 $M_{\odot} \text{ yr}^{-1}$), typically a factor of 3–6 higher than massive spheroid-like objects in the same redshift range. At $z > 1$, and more pronouncedly at $z > 1.3$, the median specific SFRs of the disks and spheroids detected by MIPS are very similar, ranging from 0.1 to 1 Gyr^{-1} (SFR=10–200 $M_{\odot} \text{ yr}^{-1}$). We estimate that massive spheroid-like galaxies may have doubled (at the most) their stellar mass from star-forming events at $z < 2$: less than 20% mass increase at $1.7 < z < 2.0$, up to 40% more at $1.1 < z < 1.7$, and less than 20% additional increase at $z < 1$. Disk-like galaxies may have tripled (at the most) their stellar mass at $z < 2$ from star formation alone: up to $\sim 40\%$ mass increase at $1.7 < z < 2.0$, and less than 180% additional increase below $z = 1.7$ occurred at a steady rate.

Subject headings: galaxies: evolution — galaxies: starburst — galaxies: elliptical — galaxies: formation — galaxies: photometry — galaxies: high-redshift — infrared: galaxies

1. INTRODUCTION

The formation and evolution of massive ($M > 10^{11} M_{\odot}$) galaxies is one of the most studied topics in extragalactic astronomy during the last decade. Early expectations from hierarchical galaxy formation models considered that star formation began in low mass systems which built more massive galaxies through sequential merging (Baugh et al. 1996; Cole et al. 2000), in a similar process to the growth of structures in Cold Dark Matter simulations (Springel et al. 2005). In apparent contradiction with hierarchical assembly, the finding of a substantial population of massive galaxies at $z > 1$ (Elston et al. 1988; Hughes et al. 1998; Franx et al. 2003; Glazebrook et al. 2004), some of them containing old stellar populations and evolving passively (according to their red optical colors –Daddi et al. 2004, Reddy et al. 2005–, and spectra –Kriek et al. 2006, 2008; Cimatti et al. 2008–), seems to favor a downsizing formation scenario (Cowie et al. 1996; Heavens et al. 2004; Juneau et al. 2005; Pérez-González et al. 2005; Bundy et al. 2006). This population of $z > 1$ massive galaxies accounts for a significant fraction of the local stellar mass density ($\sim 20\%$ as early as $z \sim 2$, and

$\sim 10\%$ at $z \sim 4$: Fontana et al. 2006; Arnouts et al. 2007; Pérez-González et al. 2008). The discovery of such a population reinforced the idea that both stars and their host galaxies are coeval (resembling a monolithic-like collapse), and consequently, no expectations of structure evolution in these galaxies should be expected. For this reason, the recent observational evidence showing that the most massive galaxies were much more compact in the past (Daddi et al. 2005; Trujillo et al. 2006; Longhetti et al. 2007; Cimatti et al. 2008) has been surprising, and has again opened the question of how the stellar populations of these galaxies were assembled into their present shape.

The size evolution of the most massive objects since $z \sim 2$ has been characterized by Trujillo et al. (2007). These authors found that, at a given stellar mass, disk-like objects at $z \sim 1.5$ were a factor of two smaller than their present-day counterparts. For spheroid-like objects, the evolution has been even stronger: they were a factor of four smaller at $z \sim 1.5$ than nearby similar mass ellipticals. In addition, the stellar mass densities of these high- z galaxies were almost two orders of magnitude higher than objects of the same mass today. These superdense galaxies have been found at even higher ($z \sim 2.5$) redshifts (Zirm et al. 2007; Toft et al. 2007; van Dokkum et al. 2008), adding more controversy to the debate about the formation and evolution of massive galaxies.

Two processes have been proposed to allow the superdense high- z galaxies migrate to the local stellar mass-size relation. The first process is dissipation-

Electronic address: pgperez@astrax.fis.ucm.es

¹ Departamento de Astrofísica, Facultad de CC. Físicas, Universidad Complutense de Madrid, E-28040 Madrid, Spain

² Associate Astronomer at Steward Observatory, The University of Arizona

³ Instituto de Astrofísica de Canarias, Vía Láctea s/n, E-38200, La Laguna, Tenerife, Spain

⁴ University of Nottingham, School of Physics & Astronomy, Nottingham NG7 2RD, UK

less (with absence of star formation) merging. Given the high metal abundances and old ages of the stellar population present in local massive elliptical galaxies (e.g., Gallazzi et al. 2006; Sánchez-Blázquez et al. 2006; Jimenez et al. 2007), these mergers should preferentially be dry (De Lucia et al. 2006), and occur between $z \sim 1.5$ and $z=0$, the epoch when the red sequence appears (Labbé et al. 2007). In this context, a particular effective size evolutionary mechanism ($r_e \sim \mathcal{M}^{1.3}$) has been provided by Boylan-Kolchin et al. (2006) through head-on mergers of galaxies. The second possibility is the smooth envelope accretion scenario (Naab et al. 2007), where accreted stars (mainly provided by minor mergers) form an envelope whose size increases smoothly at decreasing redshift.

The goal of this paper is to explore the evolutionary paths followed by the most massive galaxies and their dependence on the morphology. To do this, we quantify the growth in stellar mass via star formation events of massive ($\mathcal{M} > 10^{11} \mathcal{M}_\odot$) galaxies as a function of size and brightness profile shape up to $z \sim 2$. We base our discussion on the characterization of the dust infrared (IR) emission of these systems, which is linked to the amount of recent star formation and/or the presence of obscured AGN. This IR-based study is complementary to the more classical approach to the characterization of the evolution of massive ellipticals based on rest-frame optical properties.

Throughout this paper, we use a cosmology with $H_0 = 70 \text{ km s}^{-1} \text{ Mpc}^{-1}$, $\Omega_M = 0.3$ and $\Lambda = 0.7$. All magnitudes refer to the AB system. The results for stellar masses and SFRs assume a Chabrier (2003) initial mass function (IMF) with $0.1 < \mathcal{M} < 100 \mathcal{M}_\odot$.

2. DATA DESCRIPTION

2.1. The sample

To analyze the star formation properties of the most massive galaxies as a function of morphology, we use the catalog of 831 K -band selected massive galaxies ($\mathcal{M} > 10^{11} \mathcal{M}_\odot$) in the Palomar Observatory Wide-Field Infrared (POWIR)/DEEP-2 survey (Davis et al. 2003; Bundy et al. 2006; Conselice et al. 2008) for which Trujillo et al. (2007) provide redshifts, stellar masses, and structural parameters (sizes and Sérsic indices). These data, jointly with the *Spitzer*/MIPS fluxes measured in the observations carried out by the FIDEL Legacy Program in the Extended Groth Strip (EGS), allow a detailed analysis of the star formation properties of the most massive galaxies as a function of morphology up to $z \sim 2$.

The sample is described in detail in Conselice et al. (2007) and Trujillo et al. (2007). Briefly, the K -band survey covers 2165 arcmin^2 in the EGS and has a depth $K = 22.5 \text{ mag}$ (5σ). Only 710 arcmin^2 are covered simultaneously with HST/ACS v - and i -band imaging from the All-Wavelength Extended Groth Strip International Survey (AEGIS, Davis et al. 2007), so reliable structural parameters can only be measured for 831 galaxies within the entire POWIR/DEEP-2 survey in EGS. Half of those 831 galaxies has spectroscopic redshifts based on optical data obtained by the DEEP-2 Galaxy Redshift survey (Davis et al. 2003). Conselice et al. (2007) estimate photometric redshifts for the rest of sources

with an accuracy $\Delta z / (1+z) = 0.025$. The 831 galaxies with $\mathcal{M} > 10^{11} \mathcal{M}_\odot$ in the EGS lie in the redshift range $0.2 < z \lesssim 2$. Stellar masses were estimated by Bundy et al. (2005, 2006) using the exponential star formation models of Bruzual & Charlot (2003) with a Chabrier (2003) IMF and various ages, metallicities and dust contents included. As shown by Conselice et al. (2007), typical uncertainties in the stellar masses are a factor of ~ 2 (typical of any stellar population study; see, e.g., Pérez-González et al. 2003, Kauffmann et al. 2003, Papovich et al. 2006, Fontana et al. 2006, and Pérez-González et al. 2008). As discussed in detail in Conselice et al. (2007), this factor includes the effects of the photometric redshift uncertainties, the errors inherent to solution degeneracies, and the choices of the IMF and the stellar emission library. For example, using Maraston (2005) models (with an improved treatment of the TP-AGB stellar evolution phase) would produce a 20% (at most) systematic decrease in the mass estimations. Using a Salpeter (1955) IMF would increase the stellar masses by a constant factor of 0.25dex.

Trujillo et al. (2007) estimated (circularized) half-light radius (r_e) and Sérsic (1968) indices (n) for all the galaxies in our sample. They used i -band HST/ACS images to fit surface brightness profiles and divided the sample in disk-like and spheroid-like galaxies according to the value of the Sérsic index. Ravindranath et al. (2004, see also Andredakis et al. 1995) demonstrated that nearby galaxies with $n < 2.5$ are mostly disks, while spheroids are characterized by high Sérsic indices, $n > 2.5$. They also performed simulations to check that the Sérsic index obtained from HST data can be used as a morphology indicator at $z > 0$. Trujillo et al. (2007) extended these simulations to prove that the structural parameters are robust against the effects introduced by K -corrections, AGN contamination, and surface brightness dimming.

For our sample, visual inspection of the ACS i -band images by one of the co-authors (I.T.) was used to classify the sample in 4 types: ellipticals/lenticulars, spirals, irregulars, and mergers. Comparing this visual classification with the one based on Sérsic indices, we find that the visually confirmed spheroids present $\langle n \rangle = 4.8 \pm 1.5$, and the rest of sources have $\langle n \rangle = 1.7 \pm 1.7$. There is a 6% contamination of visually identified spheroids in the $n < 2.5$ sample, and a 20% contamination of visually identified disks in the $n > 2.5$ sample (comparable to the 5% and 19% contaminations in Ravindranath et al. 2004). The fraction of interloper disks decreases to 7% at $n > 4$ and 4% at $n > 5$. A 4% contamination is typical of other works based on visual or quantitative morphological classifications such as Conselice et al. (2007) or Bundy et al. (2005). The visual test shows that the galaxies with $n > 4$ form a robust (almost uncontaminated) sample of spheroid-like sources, and $n < 2.5$ galaxies are mostly disks. Galaxies with $2.5 < n < 4$ are most probably spheroid-like galaxies with some contamination of S0 galaxies and early-type spirals.

2.2. UV-to-MIR photometric properties of the sample

The positions of the 831 massive galaxies in the EGS were cross-correlated (using a $1''$ search radius) with our own reduction and catalogs of the *Spitzer* IRAC survey of the EGS. Using the same simulation method described in Pérez-González et al. (2008), we found that this cata-

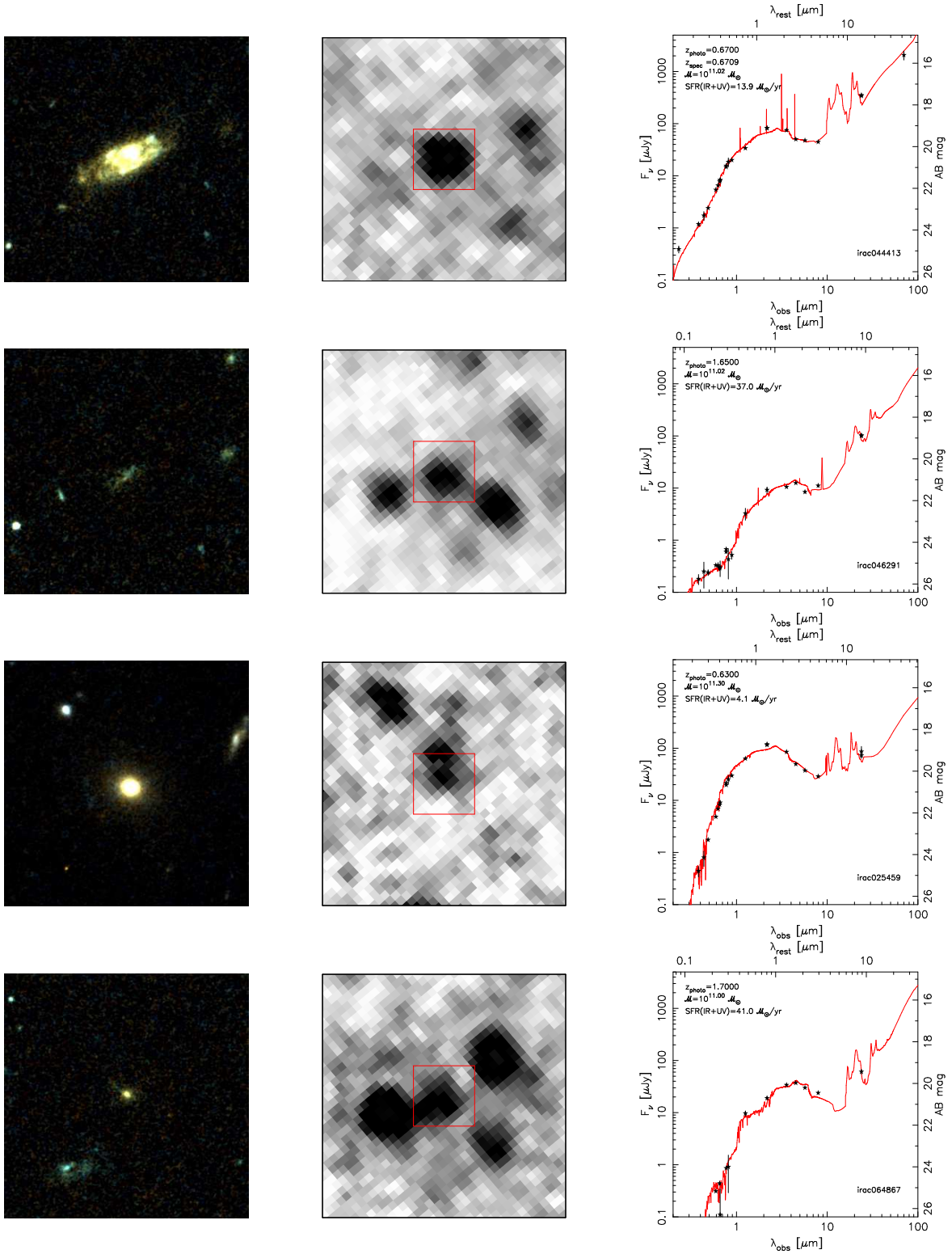


FIG. 1.— Postage stamps and SEDs for four typical MIPS-detected galaxies in our sample of massive galaxies. Left panels show $10'' \times 10''$ RGB composite images built from HST/ACS v and i frames. In the middle column, MIPS $24 \mu\text{m}$ images of size $40'' \times 40''$ are depicted, with the red square showing the area covered by the ACS postage stamp. In all images, North is up and East is left. The right columns show the SEDs of each galaxy, fitted to stellar population and dust emission models which are used to estimate photometric redshifts, stellar masses and SFRs (these parameters are given in each SED plot). The two upper rows show examples of disk-like galaxies: EGS142126.97+531137.4, a galaxy at $z=0.67$; and EGS142013.18+525925.0, lying at $z=1.65$. The two lower rows show examples of spheroid-like galaxies: EGS142021.47+525543.4, a galaxy at $z=0.63$, and EGS142125.76+531622.8, placed at $z=1.70$.

log is 75% complete at $\sim 1.5 \mu\text{Jy}$ ($[3.6]=23.5$ mag), which corresponds to 8σ detections. Our IRAC photometry is consistent with that published by Barmby et al. (2008) for the same dataset (but their own reduction and cataloging) within 0.1 mag (typical absolute uncertainty of IRAC fluxes) for 75% of the sample, and within $1-\sigma$ error for virtually all sources.

We found IRAC counterparts down to $[3.6]=23$ mag for all of the 831 galaxies in Trujillo’s sample. For 151 sources (18% of the total), the IRAC sources were blended with nearby objects, but still resolved (the separation was larger than $1''$). As described in detail in Appendix A of Pérez-González et al. (2008), for these sources we obtained multi-wavelength photometry (including *Spitzer* fluxes) using a deblending algorithm based on the deconvolution of the IRAC and MIPS images. The method takes the known positions of the blended sources obtained from optical/NIR ground-based images and the PSFs for the different images and obtain separated fluxes for the blended sources (see also Grazian et al. 2006). The method relies on the moderate resolution of the IRAC images ($\sim 2''$ FWHM, not that different from an optical ground-based image, but very stable), which allows the deblending of sources separated by more than $\sim 1''$ (half of the FWHM). For the MIPS $24 \mu\text{m}$ images, the resolution is worse ($\sim 6''$ FWHM) but the IRAC data can be used to assign most probable counterparts and help with the deblending. In any case, the main results in this paper (the MIPS detection fraction and the statistics of specific SFRs) remain virtually unchanged (less than 5% random changes at all redshifts) when we remove the 151 sources with blending problems.

We measured consistent aperture photometry in several UV, optical, NIR, and MIR bands with the method described in Pérez-González et al. (2008). The multi-wavelength dataset is outlined briefly in Villar et al. (2008) and will be characterized in detail in Barro et al. (2008, in preparation). More noticeably, our merged photometric catalog includes MIPS fluxes at $24 \mu\text{m}$ obtained from aperture photometry in the GTO and FIDEL survey (DR2) data in the AEGIS/EGS field (Davis et al. 2007; Symeonidis et al. 2007). Following the same procedure described in Pérez-González et al. (2005, 2008), we used the DAOPHOT software package in IRAF⁵ to detect sources (using a 3σ detection cut above the local sky noise) in the MIPS images and measure aperture photometry with a PSF fitting method.

Based on simulations consisting on the creation and recovery of artificial sources in these images, we found that our $24 \mu\text{m}$ catalog of the EGS is 75% complete at $35 \mu\text{Jy}$ (consistent with Papovich et al. 2004 and Treister et al. 2006). $F(24)=35 \mu\text{Jy}$ corresponds to $\sim 6\sigma$ detections for the average sky noise in the FIDEL DR2 images. Our $24 \mu\text{m}$ catalogs are cut to 3σ detections, which translate to the range 14–17 μJy , depending on the location on the sky due to small differences in exposure time and the effect of confusion (both presenting small spatial variations throughout the image). As done in Pérez-González et al. (2005), we tested the reliability of

the MIPS detections by analyzing the probability of having a counterpart within the search radius ($1''$) in other optical/NIR (ground-based and IRAC) bands for a random position on the sky of the $24 \mu\text{m}$ image. Having a counterpart in 3 different bands within the EGS dataset has a negligible probability (1.4%), so we conclude that (virtually) all the MIPS detections within our sample are not spurious. Figure 1 shows postage stamps and spectral energy distributions (SEDs) of two typical examples of disk-like galaxies and two spheroid-like galaxies detected by MIPS at $24 \mu\text{m}$ (also one $70 \mu\text{m}$ detection included).

Using the measured MIPS $24 \mu\text{m}$ fluxes, the estimated 280 nm synthetic fluxes inter/extrapolated in the spectral energy distribution fits, and the spectroscopic and photometric redshifts published by Trujillo et al. (2007), we obtained total (unobscured plus obscured) SFRs for each galaxy in the same way explained in Pérez-González et al. (2008, see also Bell et al. 2005). Briefly, the MIR fluxes at rest-frame wavelengths longer than $5 \mu\text{m}$ are fitted to dust emission models (from several libraries) and the IR-based SFRs are obtained from integrated total IR (using the calibration in Kennicutt 1998) and rest-frame $24 \mu\text{m}$ (see Alonso-Herrero et al. 2006) luminosities from the fits (averaged through all template libraries). The IR-based (obscured) SFR is then added to the UV-based (unobscured) SFR to obtain the total SFR. As discussed in that paper, total SFR estimates should be good within a factor of 2. The SFRs discussed in the following Sections were estimated assuming a Chabrier (2003) IMF, obtained by dividing the results obtained with the calibrations in Kennicutt (1998, valid for a Salpeter 1955 IMF) by a 1.8 factor.

3. RESULTS AND DISCUSSION

3.1. IR emission of the most massive galaxies at $z \lesssim 2$

Figure 2 shows the location of the MIPS detections in a stellar mass–size diagram for massive galaxies as a function of the concentration index. Out of the 831 galaxies in Trujillo’s sample of massive galaxies, 485 sources (58%) were classified as spheroid-like based on their high ($n > 2.5$) Sérsic (1968) indices, and 346 (42%) as disk-like sources ($n \leq 2.5$). Among the disk-like sources, 322 (93% of all disks) are detected by MIPS at $24 \mu\text{m}$ with a minimum flux $F(24)=15 \mu\text{Jy}$, and 137 galaxies are detected at $70 \mu\text{m}$ down to $F(70)=0.5 \text{ mJy}$. Among the spheroids, 297 galaxies (61% of the total) are detected at $24 \mu\text{m}$ down to $F(24)=14 \mu\text{Jy}$, and 84 sources are detected at $70 \mu\text{m}$ down to $F(70)=0.7 \text{ mJy}$. If we consider only the MIPS 5σ detections (i.e., more statistically reliable sources, although our simulations reveal that all our 3σ $24 \mu\text{m}$ sources are reliable to the 99% level; see Section 2.2), the MIPS detection fractions decrease to 92% for disk systems and 52% for spheroid-like sources.

Table 1 shows the total number of sources and MIPS detection fractions (for fluxes above the 3σ level) as a function of redshift and morphology. We consider the results based on the morphological classification using the Sérsic indices and the direct visual inspection of the images. The MIPS detection fractions for $n \leq 2.5$ galaxies and visually identified disks are almost identical. Visually confirmed spheroids present less MIPS detections than the $n > 2.5$ sources, although the difference is small

⁵ IRAF is distributed by the National Optical Astronomy Observatory, which is operated by the Association of Universities for Research in Astronomy (AURA), Inc., under cooperative agreement with the National Science Foundation.

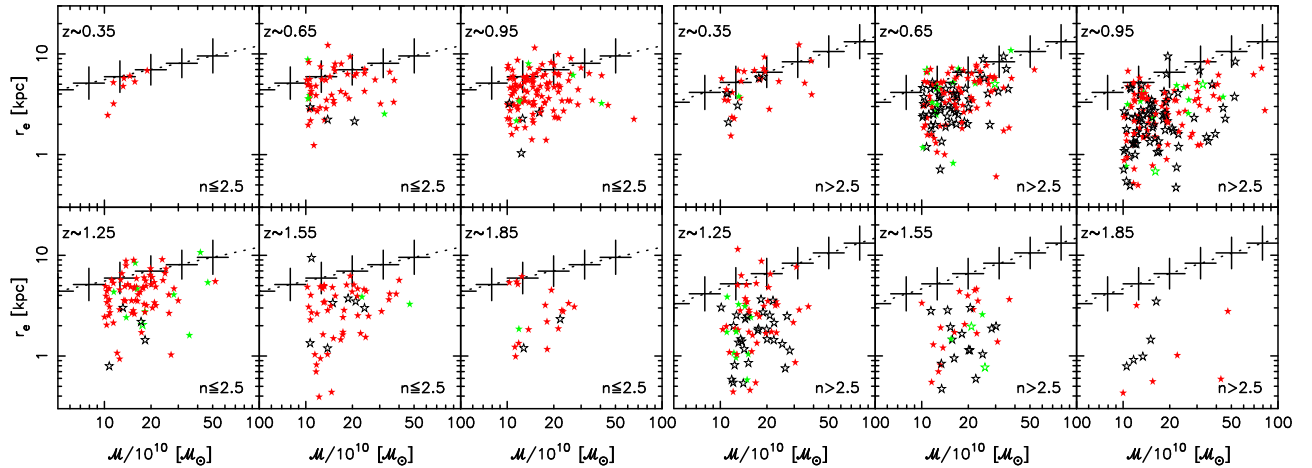


FIG. 2.— Stellar mass–size distribution for different redshift bins of our massive galaxies separated in disk-like (left panels) and spheroid-like (right panels) types. Galaxies detected by MIPS at $24\ \mu\text{m}$ are plotted with filled stars, while open stars show MIPS non-detections. Red symbols are galaxies whose MIPS emission is identified with obscured star formation, and green symbols depict galaxies which harbor an X-ray or/and IR-emitting AGN.

TABLE 1
MIPS DETECTION FRACTION AND SPECIFIC SFR STATISTICS AS A FUNCTION OF MORPHOLOGY.

Redshifts	Sérsic index classification				Visual classification			
	Sources (MIPS detected)		$\log(\text{SFR}/\mathcal{M}^\dagger)$		Sources (MIPS detected)		$\log(\text{SFR}/\mathcal{M}^\dagger)$	
	$n \leq 2.5$	$n > 2.5$	$n \leq 2.5$	$n > 2.5$	S/Irr/mergers	E/S0	S/Irr/mergers	E/S0
(0.2,0.5]	8 (100.0%)	31 (80.6%)	$-1.33_{-1.08}^{-1.57}$	$-2.03_{-1.68}^{-2.23}$	14 (100.0%)	25 (76.0%)	$-1.37_{-1.12}^{-1.68}$	$-2.12_{-2.01}^{-2.36}$
(0.5,0.8]	55 (94.5%)	144 (60.4%)	$-1.05_{-0.76}^{-1.34}$	$-1.54_{-1.22}^{-2.00}$	88 (94.3%)	111 (50.5%)	$-1.12_{-0.79}^{-1.43}$	$-1.82_{-1.46}^{-2.07}$
(0.8,1.1]	120 (95.8%)	173 (57.2%)	$-0.79_{-0.62}^{-0.99}$	$-1.59_{-1.10}^{-1.81}$	156 (95.5%)	137 (48.2%)	$-0.86_{-0.63}^{-1.06}$	$-1.63_{-1.44}^{-1.86}$
(1.1,1.4]	83 (94.0%)	83 (66.3%)	$-0.60_{-0.49}^{-0.72}$	$-0.89_{-0.66}^{-1.10}$	104 (98.1%)	62 (50.0%)	$-0.63_{-0.49}^{-0.77}$	$-1.26_{-0.90}^{-1.48}$
(1.4,1.7]	56 (87.5%)	40 (57.5%)	$-0.51_{-0.30}^{-0.72}$	$-0.61_{-0.12}^{-1.07}$	60 (86.7%)	36 (52.9%)	$-0.51_{-0.23}^{-0.77}$	$-0.61_{-0.32}^{-0.98}$
(1.7,2.0]	21 (85.7%)	12 (58.3%)	$-0.17_{+0.02}^{-0.50}$	$-0.40_{-0.13}^{-0.61}$	24 (83.3%)	9 (50.0%)	$-0.36_{+0.01}^{-0.61}$	$-0.17_{-0.06}^{-0.33}$

NOTE. — \dagger In units of Gyr^{-1} .

(<10%) and consistent with the 20% contamination of visually identified disks in the $n > 2.5$ sample, most of them having $2.5 < n < 4.0$ (see Figure 3).

Figure 2 shows that there is basically no difference between the loci occupied by MIPS detected and undetected galaxies in the stellar mass–size plane. However, for spheroid-like objects at a given stellar mass, MIPS non-detections are smaller than IR-bright sources by a factor of ~ 1.2 (see also Zirm et al. 2007 results at higher z). This suggests that early (i.e., $z > 2$) massive star formation events left even more compact remnants than starbursts taking place at $z < 2$, maybe reflecting the higher density conditions of the primitive Universe.

Figure 3 shows the MIPS $24\ \mu\text{m}$ detection fractions as a function of structural parameters. This Figure confirms the bias of the $n \leq 2.5$ sample towards galaxies with ongoing (possibly extended through the disk) star formation or harboring an IR-emitting AGN. Figure 3 demonstrates that virtually all (80–90%) the $n \leq 2.5$ galaxies are detected by MIPS at all redshifts and (almost) independently of the size of the galaxy. In contrast, the spheroid sample is biased towards more quiescent systems. There is still a non-negligible fraction (6%) of galaxies classified as disky which fall below the MIPS detection limit

or do not present any IR emission, i.e., they have low-level star formation, no dust, or are completely quiescent. According to Figure 3, most of them lie at $z > 1$ (59% of all disk-like non-detections) and tend to have comparatively smaller sizes: the MIPS detection fraction decreases from 90% for disk-like galaxies with $r_e \gtrsim 4$ kpc to 70–80% for $r_e \lesssim 1.5$ kpc systems. All these sources present very red SEDs (see Figure 4).

On the contrary, the spheroid-like sample includes at least a 63% of “active” galaxies. Moreover, some more MIPS undetected spheroids may have some star formation activity or harbor an AGN, since some of the SEDs in the upper-left panel of Figure 4 present a significant emission in the UV, probably arising from young stars. Most of these UV-bright galaxies lie at $z > 1$, and the MIPS $24\ \mu\text{m}$ flux upper limits⁶ are consistent with the MIR emission from a typical Sc galaxy. Figure 3 shows that MIPS detections are more common among the largest spheroid-like galaxies, especially at $z > 1$. Interestingly, at $z > 1$ the MIPS detection fraction stays roughly constant at $r_e \lesssim 3$ kpc. It may even increase (up to 70%)

⁶ The flux upper limits at $70\ \mu\text{m}$ have been omitted from Figure 4 for clarity, given that very few sources are detected at this wavelength.

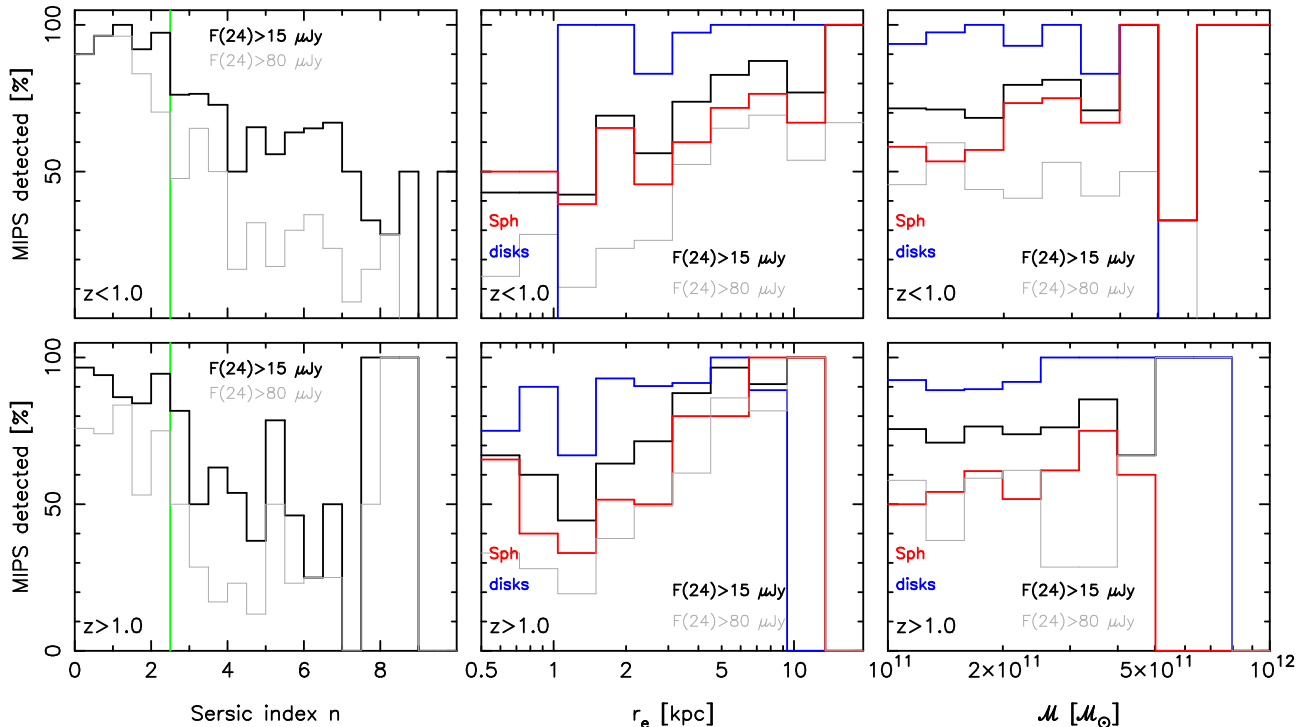


FIG. 3.— MIPS 24 μm detection fractions as a function of Sérsic index (left panels), (circularized) half-light radius (middle panels), and stellar mass (right panels). The whole sample has been divided into two redshift intervals ($z < 1$ on the top panels, and $z > 1$ on the bottom panels). Galaxies identified as IR- or X-ray-bright AGN are excluded from the distributions. In all plots, wide black lines show the results for all the MIPS detections (with a minimum measured value of $F(24) = 15 \mu\text{Jy}$) and gray narrow lines show the measured fractions for a flux cut $F(24) > 80 \mu\text{Jy}$. On the left panels, the green vertical line shows the adopted separation between spheroid-like and disk-like galaxies. On the middle and right panels, red lines show the MIPS detection fractions for spheroid-like sources, and blue lines for disk-like sources.

for very compact ($r_e \lesssim 1$ kpc) spheroid-like galaxies, although there are 3 caveats to this result: 1) the number of sources with $r_e \lesssim 1$ kpc is small (~ 30), so the uncertainties in these bins are of the order of 20-30%; 2) for $z > 1$ and $r_e \lesssim 1$ kpc we are reaching the resolution limit in the HST/ACS images, and consequently the size measurements count with large uncertainties; and 3) these high- z compact galaxies may be dominated by an obscured AGN (since the galaxies are detected by MIPS and show no X-ray emission; see also Trujillo et al. 2007), which may bias the size measurements.

Our results may be compared with those published by Rodighiero et al. (2007). They found that 20% of the most securely identified spheroids⁷ at $0.3 < z < 1.0$ are detected during phases of prominent activity. The evidence is the detection at 24 μm above $80 \mu\text{Jy}$ or at radio wavelengths above $40 \mu\text{Jy}$. Our MIPS data are deeper than theirs, but if we cut our catalogs to the same flux limit (see Figure 3), we obtain an average $\sim 20\%$ detection fraction at $z < 1$ for the most concentrated objects with $n > 4$, probably well correlated with their sample of bona fide spheroids, although our selection only includes the most massive galaxies ($M > 10^{11} M_\odot$), and Rodighiero’s selection is not based on stellar mass.

If we consider the high- z ($z > 1$) galaxies in our sample, our results are also consistent with those found in Papovich et al. (2006) for Distant Red Galaxies (DRGs).

These galaxies have a typical stellar mass $M \sim 10^{11} M_\odot$ and a mean redshift $z \sim 2$ (see also Grazian et al. 2007; Pérez-González et al. 2008). Given that our sample has a stellar mass cut $M > 10^{11} M_\odot$ and a redshift cut at $z = 2$, the low-redshift, high-mass tail of the general DRG population must be included in our selection. Indeed, we have 27 DRGs in our sample, with an average redshift $\langle z \rangle = 1.50 \pm 0.22$. Papovich et al. (2006) found that roughly 50% of DRGs are detected by MIPS at 24 μm down to $80 \mu\text{Jy}$. We find a $\sim 60\%$ detection fraction for massive galaxies in the low redshift tail of DRGs ($1 < z < 2$) with deeper data (75% completeness level at $35 \mu\text{Jy}$). Among the 27 DRGs in our sample, 25 (93%) are detected by MIPS. This detection fraction is higher than the average for $1 < z < 2$ galaxies, but still consistent with the results in Papovich et al. (2006), who argue that $z \lesssim 2$ DRGs are mostly heavily extinguished starbursts part of the class of dusty EROs at $z > 1$, and find a $\sim 75\%$ MIPS detection fraction for their $M > 10^{11} M_\odot$ DRGs at $z < 2$. Indeed, 18 DRGs in our sample are EROs (16 MIPS detections), and we count with a total of 305 EROs in our entire sample.

3.2. Spectral energy distributions

Figure 4 shows the SEDs of all the massive galaxies in our EGS sample divided into morphological and activity types. The two panels on the right show the SEDs for galaxies with an X-ray detection (Barmby et al. 2006, Nandra et al. 2007; see also Conselice et al. 2007) or classified as IRAC power-law galaxies (PLGs, Donley et al. 2007), i.e., sources which most probably harbor an X-ray

⁷ Note that Rodighiero et al. (2007) cut their sample to clear E and E/S0 galaxies as classified visually by Bundy et al. (2005), but do not include Bundy’s S0 type in their analysis.

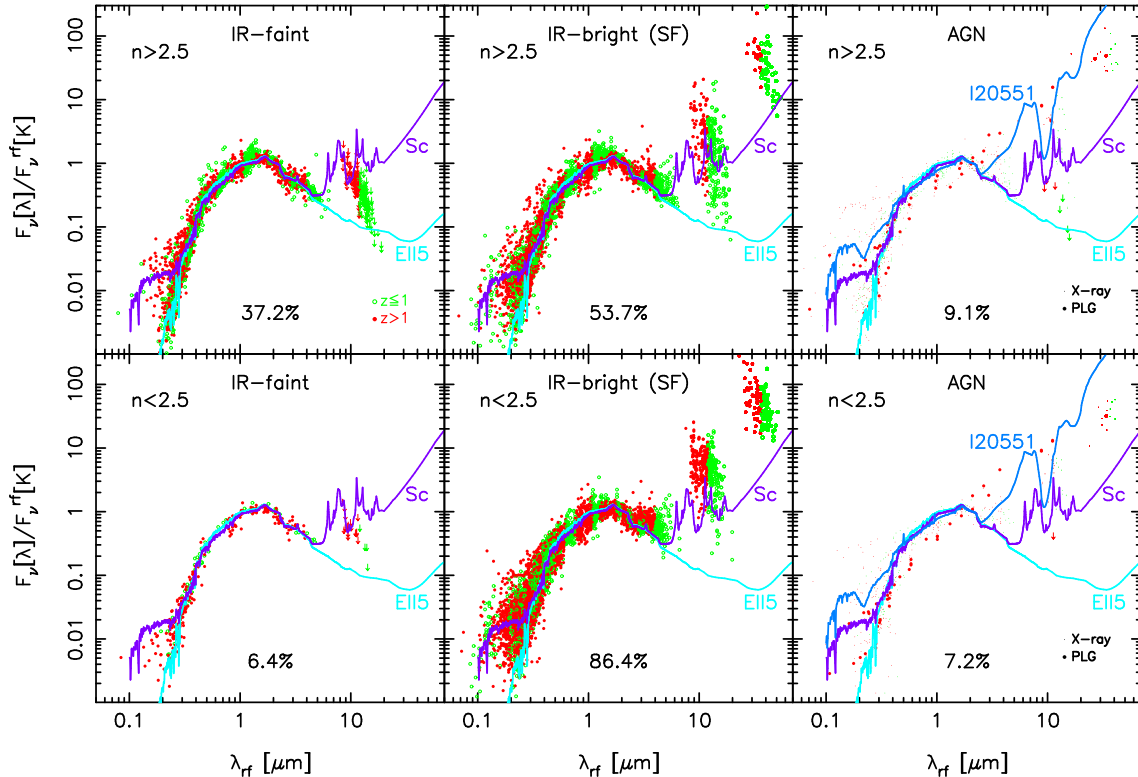


FIG. 4.— Spectral energy distributions (de-redshifted and normalized to the rest-frame K -band flux) of all the galaxies in the sample of massive galaxies ($M > 10^{11} M_{\odot}$) in the EGS (Trujillo et al. 2007). The upper and lower panels show the SEDs for the spheroid-like and disk-like galaxies, respectively. For each morphological type, the sub-sample has been divided in three groups: galaxies without MIPS detection (IR-faint, left panels, with arrows showing an upper limit of the MIPS $24 \mu\text{m}$ emission corresponding to $15 \mu\text{Jy}$, the minimum flux observed in the sample⁵), galaxies with a MIPS counterpart most probably linked to on-going star formation (IR-bright, middle panels), and galaxies with nuclear activity (AGN, right panels, see text for details). In each panel, open green circles show sources at $z < 1$, and filled red circles depict galaxies at $1 < z < 2$. We also show typical templates (from Polletta et al. 2007) of an elliptical galaxy (E115), a late-type spiral galaxy (Sc), and a galaxy with an obscured AGN (I20551, just for the AGN panels on the right). All panels show the fraction of sources in each type for the spheroid-like and disk-like samples.

and/or IR emitting AGN. There are 68 X-ray emitters, 60 of them with MIPS detection, and 5 PLGs in total, all of them with X-ray emission and 4 with MIPS emission.

The SED distribution of the spheroids present a lower scatter in the UV/optical, being very similar to a spectral template of an elliptical. In contrast, there is a very populated tail of disk-like galaxies with UV/optical fluxes brighter than a template for a typical Sc galaxy, most probably linked to a recent starburst. The MIR emission is consistent with the PAH spectrum of a late-type spiral galaxy (see also Figure 1), but can be as high as 6–10 times the flux of the Sc template from Polletta et al. (2007). Spheroid-like galaxies with a MIPS detection present a lower $24 \mu\text{m}$ median flux ($82 \mu\text{Jy}$, with the quartiles being $42 \mu\text{Jy}$ and $188 \mu\text{Jy}$, and the average $160 \mu\text{Jy}$) than MIPS disk sources ($190_{107}^{301} \mu\text{Jy}$, and the average $250 \mu\text{Jy}$). Most of the sources identified as AGN present relatively bright fluxes at rest-frame wavelengths between 2 and $10 \mu\text{m}$, revealing the presence of very hot dust heated by the central supermassive black hole and emitting in the NIR and MIR. In several cases, this NIR/MIR emission hides the $1.6 \mu\text{m}$ bump, typically seen in galaxies whose spectrum is dominated by stars rather than dust.

3.3. Specific Star Formation Rates

Figure 5 shows the specific SFRs of massive galaxies as a function of redshift and morphology. Table 1 gives the median and quartiles for different redshift ranges and morphological types (obtained from Sérsic index and visual classifications). The median specific SFRs increase by less than 0.1dex and 0.02dex for spheroids and disks, respectively, when considering MIPS $24 \mu\text{m}$ detected above the 5σ level. These increments do not affect the following results significantly.

When segregating the sample based on the Sérsic indices, we find that the specific SFRs of spheroid galaxies evolve as $(1+z)^{5.5 \pm 0.6}$ from $z=0$ to $z=2$, while the evolution for disk-like galaxies goes as $(1+z)^{3.6 \pm 0.3}$. If we consider the results based on the visual classification, the evolution is more pronounced for spheroids and almost identical for disks: $(1+z)^{6.4 \pm 0.8}$ evolution for the former, and $(1+z)^{3.4 \pm 0.2}$ for the latter.

The specific SFRs used in Figure 5 have been estimated by adding the unobscured SFRs obtained from UV data (at rest-frame 280 nm) and the obscured SFRs from IR data (using the total IR luminosity) as explained in Pérez-González et al. (2008). The ratio between these two quantities allow the estimation of the global obscuration of the recent star formation in each galaxy (only for those detected by MIPS). On average, we find that extinctions for MIPS detected galaxies increase

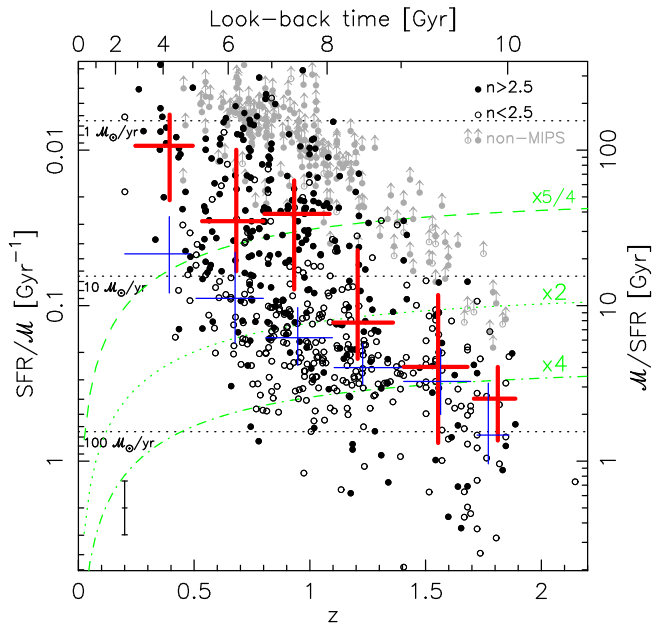


FIG. 5.— Specific SFRs as a function of redshift and morphology (for galaxies not identified as bright AGN). Galaxies detected at $24\ \mu\text{m}$ are plotted with open (disks) and filled (spheroids) black circles, while gray symbols show upper limits for sources not detected by MIPS. Red and blue crosses represent the median and quartiles for the distribution of specific SFRs in the different redshift ranges used in Trujillo et al. (2007, red widest lines referring to spheroids and blue narrowest to disk-like galaxies). Green curves show the expected positions of galaxies which would multiply their stellar mass by $5/4$, 2 , and 4 between their redshift and $z=0$ if they maintained a constant SFR. Horizontal dashed lines show constant SFR values for the median stellar mass of our sample ($1.6 \times 10^{11}\ M_{\odot}$).

with redshift, ranging from $\langle A(V) \rangle = 1.0 \pm 0.5$ mag at $z < 0.5$ to $\langle A(V) \rangle = 1.5 \pm 0.6$ mag at $z \sim 1$ and $\langle A(V) \rangle = 2.0 \pm 0.7$ mag at $z \sim 2$. These values are consistent with typical attenuations found for IR-bright galaxies by, e.g., Rigopoulou et al. (2000), and the evolution in the extinction properties of the UV SFR density found by Tresse et al. (2007). According to Symeonidis et al. (2007), even larger extinctions (up to a factor of ~ 100) are needed to match SFRs obtained from IR or radio data and SFRs obtained from [OII] spectroscopic observations of IR-bright sources in the EGS.

Figure 5 shows that below $z=1.1$ spheroid-like galaxies present very low specific SFRs. On average, they would increase their stellar mass by less than 25% at $0 < z < 1$ if they maintained a constant SFR. The global mass increase (in the form of newly-formed stars) for all spheroid-like galaxies is less than 10% if we take into account the 38% of $z < 1$ spheroids which are not detected by MIPS, and even lower ($\sim 5\%$) if we only consider the visually identified spheroids. In contrast, disk-like galaxies could typically double their mass from $z=1$ to $z=0$ due to newly formed stars if they maintained a constant SFR, with little change due to the very few galaxies (less than 5%) for which we only have SFR upper limits.

In practice, IR-bright intense star-forming bursts are not expected to last long (Mihos & Hernquist 1994), so a galaxy most probably will not maintain a high SFR level for several Gyr. The higher SFR values are expected to be maintained for shorter periods, since gas exhaustion and supernova winds (and even AGN activity) will help

to suppress star formation. Mihos & Hernquist (1996) simulations of mergers predict the triggering of a very intense and short starburst event (probably detectable in the MIR by MIPS) lasting a few tens of Myr (and occurring in late stages of the merger, when the galaxies are actually joining) for encounters of galaxies with an already formed bulge. Encounters of disk galaxies would trigger less intense bursts lasting longer (100-200 Myr) and occurring earlier in the merger process. For the observed specific SFRs in our sample, those short and intense starbursts would add up less than 0.01% (for each merging event) to the total stellar mass of a typical spheroid-like galaxy at $z < 1$. This very small fraction of young stars would be hidden by the predominant old stellar population and be undetectable in local ellipticals. For the disk galaxies at $z < 1$, which present specific SFRs as high as $0.2\ \text{Gyr}^{-1}$, the burst strength (ratio of the newly formed stars to the global stellar mass) could be as high as a few percent (for each merging event), typical for star-forming galaxies at low-redshifts (Kauffmann et al. 2003; Pérez-González et al. 2003).

At $z \gtrsim 1$, the specific SFRs of massive galaxies are higher than $0.1\ \text{Gyr}^{-1}$, both the active spheroid-like (note that there are 40% of spheroids which are not detected by MIPS) and disk systems are forming stars at approximately the same rate, and the number of quiescent galaxies (those not detected by MIPS) is less than $\sim 50\%$ for both types. It is interesting to notice that most galaxies (disks and spheroids) have significant amounts of dust, since they are detected at $24\ \mu\text{m}$. If some of these galaxies are the progenitors of nearby ellipticals, that dust should have disappeared somehow or it is now very cold and may only be detected at very long wavelengths ($\lambda > 100\text{-}200\ \mu\text{m}$) and low fluxes.

For typical burst durations, and even for star-forming events with a constant SFR and lasting up to 1 Gyr, the maximum increase in stellar mass would be $\sim 15\%$ at $1.1 < z < 1.4$, $\sim 25\%$ at $1.4 < z < 1.7$, and $\sim 50\%$ at $1.7 < z < 2.0$, for both spheroids and disks. This means that a significant fraction (more than 50%) of the stellar mass of $z > 1$ massive galaxies was assembled at $z > 2$ (Pérez-González et al. 2008; see also Bauer et al. 2005, Feulner et al. 2005, Papovich et al. 2006). Moreover, we find that about 40% of spheroids at $z \sim 1.8$ are almost “dead” (they present low SFR levels based on IR and UV data) and evolving passively, or may be experiencing a quiescent period. Note that most spheroid-like galaxies at $z > 1$ would be qualified as passive based on optical colors alone, but the MIPS data reveals that $\sim 50\%$ of them are experiencing dusty starbursts and 10% more harbor (also) obscured AGN.

We can estimate how much stellar mass galaxies typically assemble through star formation from $z=2$ to the present (i.e., the star formation efficiency to increase the mass of a galaxy in the last 10 Gyr) if a galaxy follows the specific SFR evolution depicted in Figure 5. We assume that the SFRs remain constant within each redshift interval; since the starbursts probably last 50-200 Myr, as discussed earlier, the following figures would be an upper limit. Adding all the mass formed from $z=2$ to $z \sim 0$, we estimate that a disk-like galaxy could increase its stellar mass by up to a factor of 3.2 ± 0.5 in the last 10 Gyr: 1.4 times increase at $1.7 < z < 2.0$ and an almost constant 10-20% increase in each of our 5 redshift inter-

vals at $z < 1.7$. A spheroid-like galaxy could increase its stellar mass by up to a factor of 1.8 ± 0.3 : 1.2 times increase at $1.7 < z < 2.0$, 10-20% in each of our two intervals at $1.1 < z < 1.7$ and less than 5% in each of the three intervals at $z < 1.1$. These figures are almost unchanged ($< 5\%$ increases) when considering only the MIPS $24 \mu\text{m}$ 5σ detections. For visually identified disks and spheroids, the stellar mass increases by up to a factor of 2.7 ± 0.4 and 1.8 ± 0.3 , respectively.

Ideally, one would like to disentangle what is the relative contribution to the size growth of a galaxy of newly-formed stars and system heating through merger/interactions. However, both processes are probably linked, since new star formation events are likely associated to the interactions that could inject energy to the systems. Consequently, a definitive answer to the problem of how galaxies grow require the help of elaborate modelling. It is worth saying, nonetheless, that both the observations at low and high- z show that galaxies have larger effective radii when observed in bluer bands. This means that younger stars are preferentially located at larger galactocentric distances than older populations. In this paper, we have quantified how much the stellar mass grows through star formation events only. Once we reach a clear picture of how the galaxies can increase in size through mergers, our results will constrain the amount of stellar mass due to dry accretion that is necessary to migrate the high- z galaxies to the local size-mass relations.

4. SUMMARY AND CONCLUSIONS

We have analyzed the stellar mass growth in the form of newly-born stars in a sample of 831 K -band selected massive galaxies ($M > 10^{11} M_{\odot}$) as a function of structural parameters (size and concentration). These galaxies lie in the redshift range between $z=0.2$ and $z \sim 2$. Our analysis is based on the measurement of the specific SFR for each galaxy based on their UV and IR emission, taking advantage of the deep *Spitzer* data obtained by the FIDEL *Spitzer*/MIPS Legacy Project in the Extended Groth Strip.

Our main results follow:

- Most (more than 85% at any redshift) disk-like galaxies (identified by small Sérsic indices, $n < 2.5$) are detected by MIPS at $24 \mu\text{m}$ down to $F(24) = 15 \mu\text{Jy}$ with a median flux $F(24) = 190 \mu\text{Jy}$.
- A significant fraction (more than 55% at any redshift) of spheroid-like galaxies is detected at $24 \mu\text{m}$ down to $F(24) = 14 \mu\text{Jy}$ with a median flux $F(24) = 82 \mu\text{Jy}$.

- The MIPS detection fraction for spheroid-like galaxies is higher (70–90%) for larger ($r_e \gtrsim 5$ kpc) galaxies, especially at $z > 1$, where the detection fraction has a minimum around 30–40% for galaxies with $r_e \sim 1$ kpc. No clear trend is found for disk galaxies of different sizes.
- There is basically no difference between the loci occupied by MIPS detected and undetected galaxies in the stellar mass–size plane. However, for spheroid-like objects at a given stellar mass, MIPS non-detections are smaller than IR-bright sources by a factor of ~ 1.2 .
- Most of the galaxies in our sample present spectral energy distributions which are consistent with an elliptical template in the UV/optical/NIR spectral range. Some galaxies morphologically classified as spheroids have UV emission tails which are typical of star-forming systems, most commonly at $z > 1$.
- A $\sim 10\%$ fraction of the massive galaxies in our sample present X-ray or power-law-like mid-IR emission which must be linked to the presence of a bright (unobscured or obscured) AGN.
- Based on the measured specific SFRs, we estimate that spheroid-like galaxies have doubled (at the most, depending on the burst durations) their stellar mass due to newly-born stars alone from $z \sim 2$ to $z = 0.2$. Most of these mass increase (60%) occur at $z \gtrsim 1$, where specific SFRs are as high as 0.4 Gyr^{-1} .
- Disk-like galaxies have tripled (at the most) their stellar mass by newly-formed stars at $z < 2$, with a more steady growth rate as a function of redshift.

We thank an anonymous referee for her/his very constructive comments. We acknowledge support from the Spanish Programa Nacional de Astronomía y Astrofísica under grants AYA 2006–02358 and AYA 2006–15698–C02–02. This work is based in part on observations made with the *Spitzer* Space Telescope, which is operated by the Jet Propulsion Laboratory, Caltech under NASA contract 1407. PGP-G and IT acknowledge support from the Ramón y Cajal Program financed by the Spanish Government and the European Union.

REFERENCES

- Alonso-Herrero, A., Rieke, G. H., Rieke, M. J., Colina, L., Pérez-González, P. G., & Ryder, S. D. 2006, *ApJ*, 650, 835
 Andredakis, Y. C., Peletier, R. F., & Balcells, M. 1995, *MNRAS*, 275, 874
 Arnouts, S. et al. 2007, *A&A*, 476, 137
 Barmby, P. et al. 2006, *ApJ*, 642, 126
 Barmby, P., Huang, J. ., Ashby, M. L. N., Eisenhardt, P. R. M., Fazio, G. G., & Wright, E. L. 2008, *astro-ph/0803.0748*
 Bauer, A. E., Drory, N., Hill, G. J., & Feulner, G. 2005, *ApJ*, 621, L89
 Baugh, C. M., Cole, S., & Frenk, C. S. 1996, *MNRAS*, 283, 1361
 Bell, E. F. et al. 2005, *ApJ*, 625, 23
 Boylan-Kolchin, M., Ma, C.-P., & Quataert, E. 2006, *MNRAS*, 369, 1081
 Bruzual, G., & Charlot, S. 2003, *MNRAS*, 344, 1000
 Bundy, K., Ellis, R. S., & Conselice, C. J. 2005, *ApJ*, 625, 621
 Bundy, K. et al. 2006, *ApJ*, 651, 120
 Chabrier, G. 2003, *ApJ*, 586, L133
 Cimatti, A. et al. 2008, *A&A*, 482, 21
 Cole, S., Lacey, C. G., Baugh, C. M., & Frenk, C. S. 2000, *MNRAS*, 319, 168
 Conselice, C. J. et al. 2007, *MNRAS*, 381, 962

- Conselice, C. J., Bundy, K., U, V., Eisenhardt, P., Lotz, J., & Newman, J. 2008, *MNRAS*, 383, 1366
- Cowie, L. L., Songaila, A., Hu, E. M., & Cohen, J. G. 1996, *AJ*, 112, 839
- Daddi, E., Cimatti, A., Renzini, A., Fontana, A., Mignoli, M., Pozzetti, L., Tozzi, P., & Zamorani, G. 2004, *ApJ*, 617, 746
- Daddi, E. et al. 2005, *ApJ*, 626, 680
- Davis, M. et al. 2003, in Presented at the Society of Photo-Optical Instrumentation Engineers (SPIE) Conference, Vol. 4834, Discoveries and Research Prospects from 6- to 10-Meter-Class Telescopes II. Edited by Guhathakurta, Puragra. Proceedings of the SPIE, Volume 4834, pp. 161-172 (2003)., ed. P. Guhathakurta, 161–172
- Davis, M. et al. 2007, *ApJ*, 660, L1
- De Lucia, G., Springel, V., White, S. D. M., Croton, D., & Kauffmann, G. 2006, *MNRAS*, 366, 499
- Donley, J. L., Rieke, G. H., Pérez-González, P. G., Rigby, J. R., & Alonso-Herrero, A. 2007, *ApJ*, 660, 167
- Elston, R., Rieke, G. H., & Rieke, M. J. 1988, *ApJ*, 331, L77
- Feulner, G., Gabasch, A., Salvato, M., Drory, N., Hopp, U., & Bender, R. 2005, *ApJ*, 633, L9
- Fontana, A. et al. 2006, *A&A*, 459, 745
- Franx, M. et al. 2003, *ApJ*, 587, L79
- Gallazzi, A., Charlot, S., Brinchmann, J., & White, S. D. M. 2006, *MNRAS*, 370, 1106
- Glazebrook, K. et al. 2004, *Nature*, 430, 181
- Grazian, A. et al. 2006, *A&A*, 449, 951
- . 2007, *A&A*, 465, 393
- Heavens, A., Panter, B., Jimenez, R., & Dunlop, J. 2004, *Nature*, 428, 625
- Hughes, D. H. et al. 1998, *Nature*, 394, 241
- Jimenez, R., Bernardi, M., Haiman, Z., Panter, B., & Heavens, A. F. 2007, *ApJ*, 669, 947
- Juneau, S. et al. 2005, *ApJ*, 619, L135
- Kauffmann, G. et al. 2003, *MNRAS*, 341, 33
- Kennicutt, R. C. 1998, *ARA&A*, 36, 189
- Kriek, M. et al. 2008, *ApJ*, 677, 219
- . 2006, *ApJ*, 649, L71
- Labbé, I. et al. 2007, *ApJ*, 665, 944
- Longhetti, M. et al. 2007, *MNRAS*, 374, 614
- Maraston, C. 2005, *MNRAS*, 362, 799
- Mihos, J. C., & Hernquist, L. 1994, *ApJ*, 431, L9
- . 1996, *ApJ*, 464, 641
- Naab, T., Johansson, P. H., Ostriker, J. P., & Efstathiou, G. 2007, *ApJ*, 658, 710
- Nandra, K. et al. 2007, *ApJ*, 660, L11
- Pérez-González, P. G., Gil de Paz, A., Zamorano, J., Gallego, J., Alonso-Herrero, A., & Aragón-Salamanca, A. 2003, *MNRAS*, 338, 525
- Pérez-González, P. G. et al. 2005, *ApJ*, 630, 82
- . 2008, *ApJ*, 675, 234
- Papovich, C. et al. 2004, *ApJS*, 154, 70
- . 2006, *ApJ*, 640, 92
- Polletta, M. et al. 2007, *ApJ*, 663, 81
- Ravindranath, S. et al. 2004, *ApJ*, 604, L9
- Reddy, N. A., Erb, D. K., Steidel, C. C., Shapley, A. E., Adelberger, K. L., & Pettini, M. 2005, *ApJ*, 633, 748
- Rigopoulou, D. et al. 2000, *ApJ*, 537, L85
- Rodighiero, G. et al. 2007, *MNRAS*, 376, 416
- Salpeter, E. E. 1955, *ApJ*, 121, 161
- Sánchez-Blázquez, P., Gorgas, J., Cardiel, N., & González, J. J. 2006, *A&A*, 457, 809
- Sérsic, J. L. 1968, *Atlas de galaxias australes (Cordoba, Argentina: Observatorio Astronomico, 1968)*
- Springel, V. et al. 2005, *Nature*, 435, 629
- Symeonidis, M. et al. 2007, *ApJ*, 660, L73
- Toft, S. et al. 2007, *ApJ*, 671, 285
- Treister, E. et al. 2006, *ApJ*, 640, 603
- Tresse, L. et al. 2007, *A&A*, 472, 403
- Trujillo, I., Conselice, C. J., Bundy, K., Cooper, M. C., Eisenhardt, P., & Ellis, R. S. 2007, *MNRAS*, 382, 109
- Trujillo, I. et al. 2006, *MNRAS*, 373, L36
- van Dokkum, P. G. et al. 2008, *ApJ*, 677, L5
- Villar, V., Gallego, J., Pérez-González, P. G., Pascual, S., Noeske, K., Koo, D. C., Barro, G., & Zamorano, J. 2008, *ApJ*, 677, 169
- Zirm, A. W. et al. 2007, *ApJ*, 656, 66